Time-Domain Impedance Boundary Condition Implementation in a CFD Solver and Validation against Experimental Data of Acoustical Liners

Loris Casadei, Hugues Deniau, Estelle Piot, Thomas Node-Langlois

TIME-DOMAIN IMPEDANCE BOUNDARY CONDITION IMPLEMENTATION IN A CFD SOLVER AND VALIDATION AGAINST EXPERIMENTAL DATA OF ACOUSTICAL LINERS

Loris Casadei[1,2] **Hugues Deniau**[2] **Estelle Piot**[2]
Thomas Nodé-Langlois[1]
[1] Airbus Operations S.A.S., 31060 Toulouse, France
[2] ONERA - The French Aerospace Lab, F-31055, Toulouse, France
loris.l.casadei@airbus.com

ABSTRACT

Acoustical liners are one of the main solutions to reduce noise in modern aircraft turbofan engines. Numerical analysis such as computational aeroacoustics proved to be an accurate and reliable tool for predicting liners performance. The *impedance* (or, in another form, *reflection coefficient*) parameter is used to evaluate the acoustic absorption capability of a surface. As the impedance is a frequency dependent variable and defined based on acoustic quantities, its calculation is a difficult challenge for traditional CFD solvers, which are time-domain based and encompass both acoustic and hydrodynamic fluctuating quantities. Recent works allowed a new representation of the impedance under the form of a fractional multi-poles Time-Domain Impedance Boundary Condition (TDIBC) with a reflection coefficient formulation. The present work deals with the implementation of such TDIBC in a Finite-Volume CFD solver, with particular attention to confine the additional computational cost. Multiple validations against analytic (1D) and experimental (2D) data confirm the excellent reproduction of the noise reduction achieved by the lined wall.

1. INTRODUCTION

Aircraft noise is considered as a high-profile issue when dealing with aviation marketing attractiveness and public opinion in the air traffic development. In modern aircraft, noise sources are mostly due to landing gear, high-lift systems and engine. Concerning the engine, the major noise contributor is the fan, which in the next engine generation with ultra-high bypass ratio could be responsible for up to 70% of the overall engine noise in take-off conditions. The main technical solution to acoustic problems in turbofan engines is to cover specific noisy structures with sound-absorbing materials, named "liners". Since their introduction in industrial application, acoustical liners have been object of severe studying and improvement. The simple structure of the Ceramic Tubular (CT) liner made it a prominent tool for academic and benchmark validations. It consists of an array of narrow cavities backed by a hard wall at one end, then acting as a quarter-wavelength resonator with significant visco-thermal losses at the cavity walls. Arrays of wider cavities with addition of a perforated sheet on top creates the currently widespread Single Degree Of Freedom (SDOF) liner, which see most of its sound absorption due to resonance at specific frequencies and globally enhanced by visco-thermal losses through the short perforations. Fan inlet and bypass ducts are typical regions object of acoustical lining with SDOF liners. Manufacturing and testing of liners is a time consuming and expensive practice, reason why an appropriate numerical approach is fundamental for the design. Computational AeroAcoustics (CAA) is a deep and complex subject of research still under the reflector of many industries and laboratories. The dependency of acoustic physics to the frequency domain always posed a complication when coupling it with classical Computational Fluid Dynamics (CFD) simulations in time-domain. In order to numerically reproduce the sound absorption mechanism of a lined wall, Impedance Boundary Conditions (IBC) have been developed. Broadband Time-Domain IBC (TDIBC), capable of both capturing complicated acoustic physics and being coupled to a classical time domain solver, have been a challenging topic for the last two decades. First attempts emerged with the work of Tam and Auriault [1], then followed by different models, based on physical parameters [2–5] or on numerical multi-poles schemes [6–9]. Models combining physics and multi-poles appeared in the last decade [10, 11]. In particular, the recent work of Monteghetti [12, 13] provides a reliable modelling based on a mathematical technique referred to as the *Oscillatory-Diffuse Representation* (ODR), which adopts auxiliary differential equations to model the lined wall effect and relies directly on the liner's geometry. This approach is currently validated for linear liners, where the impedance is independent of the acoustic level; preliminary studies have investigated how to extend the model to the non-linear response of the material, without extended validation at this stage.
TDIBC have been initially developed in the framework of CAA, in the simulation of (linearized) Euler equations. Applying them to CFD solvers is a challenging task. An example for impedance laws with a simple dynamics, such as the damped Helmholtz oscillator, is brought in [14] on a multipole model applied to a delayed reflection [15]. A first successful implementation of the fully broadband

ODR model has been recently achieved with a Spectral-Difference CFD code [16]. A Finite-Volume (FV) approach has been tested in [17], where Linearized Navier-Stokes equations (on time and frequency domains) and Large Eddy Simulations (LES) codes used the impedance condition of [1] to reproduce an experimental data set, however demanding either a cumbersome formulation relying on two solvers or heavy calculation times due to the fine grid requirements of a LES. The all-new work from Shur *et al.* [18] introduces, in a FV solver, a purely numerical multipole TDIBC model derived as extension from Dragna's [19], thus using Auxiliary Derived Equations to surround the convolution problem. After a benchmark validation, they successfully assessed its capabilities on noise absorption of a turbofan scaled geometry.
In the present work, a Navier-Stokes Characteristic Boundary Condition (NSCBC) type of acoustic treatment has been implemented with an ODR in the FV Euler and Navier-Stokes CFD solver *elsA* , jointly owned by Airbus, Safran and ONERA. From an aeronautical business point view, its capability to simulate the attenuation of broadband noise phenomenae makes it a valuable choice when building an industrial numerical method and its associated tools. The paper is structured as follows. First, nods on liner's acoustic theory and time domain modeling are given, as well as a resume of the ODR method. The NSCBC approach is reviewed, from which the TDIBC is derived and implemented in the CFD solver. CFD validation is carried on a mono- and bi-dimensional cases against benchmark data. Conclusive remarks on the achieved results and expected advancements conclude the paper.

2. ACOUSTIC LINER MODELING

2.1 Impedance Definition

The acoustic concept determining the capability of a surface of reducing sound level is called *impedance*, defined as the ratio between pressure fluctuations p' and wall-normal velocity fluctuations u'_n in the frequency domain:

$$\hat{Z}(\mathbf{x},\omega) = \frac{\hat{p}'(\mathbf{x},\omega)}{\hat{u}'_n(\mathbf{x},\omega)} \tag{1}$$

being $\hat{\square}$ a generic variable in the frequency domain, $\mathbf{x}$ the location vector and ω the angular frequency. A similar parameter, here named "reflection coefficient", can be derived from (1) and it reads:

$$\hat{\beta} = \frac{\hat{Z} - \rho_0 c_0}{\hat{Z} + \rho_0 c_0} \tag{2}$$

being ρ_0 and c_0 relatively the density and speed of sound of the medium. An alternative formulation reads:

$$\hat{\beta} = \frac{\hat{z} - 1}{\hat{z} + 1} \tag{3}$$

with $\hat{z} = \hat{Z}/z_0$ the non-dimensional impedance ($z_0 = \rho_0 c_0$ is the medium characteristic impedance).

2.2 Time-Domain Impedance Representation

Regardless its natural belonging to the frequency domain, it is convenient to translate the impedance (or reflection coefficient) operator in the time domain, so that it can be coupled with classical numerical fluid simulations. This conversion reveals to be cumbersome, as instantaneous pressure depends on the convolution product:

$$p(t) = Z \star u_n(t) \tag{4}$$

To this end, various time-domain models have been proposed either to simplify or surround the convolution problem. Among the most recurrent categories are:

- rational multi-parameter, single polynomial or fractional models characterized by coefficients linked to the liner's physics (resistance, reactance, ...) [1–5]. They are of easy translation in time-domain but limited in the frequency range able to reproduce;
- numerical models, sum of elementary dynamical systems of first and second order obtained through mathematical approximations, hence losing physical meaning [6–9]. Their capability of capturing broadband signals is countered by the need of solving expensive convolution products and storing an accumulator.

The modified Extended Helmholtz Resonator (mEHR) [5] is a suitable physical model when dealing with CT or SDOF liners. It expresses the physics through coefficients linked to the perforations and cavities geometry of the liner:

$$Z_{mEHR}(s) = \overbrace{\frac{1}{\sigma_p}(a_0 + a_{\frac{1}{2}}\sqrt{s} + a_1 s) + }^{\text{perforation}} + \underbrace{\frac{1}{\sigma_c}\coth(b_0 + b_{\frac{1}{2}}\sqrt{s} + b_1 s)}_{\text{cavity}} \tag{5}$$

where s is the Laplacian variable, which can be related to the angular frequency by: $s = j\omega$, with $j = \sqrt{-1}$. The perforated sheet porosity is σ_p and the cavity porosity σ_c, which can be supposed unitary. The parameters a_i and b_i are the linking object to liner's geometry and can find different formulations. More generally, the a_0, b_0 coefficients are linked to frequency-independent losses, $a_{1/2}, b_{1/2}$ to frequency-dependent viscous-thermal losses and a_1, b_1 to mass reactance effects on phase shift. Herein, the coefficient sets proposed by Bruneau [20] and Crandall [21] are used. Such coefficients can also be optimized (through techniques like least-square fitting) to fit an experimental data set.
It has been demonstrated that the impedance model (5) accepts an Oscillo-Diffusive Representation [12, 13]. For the sake of brevity, the reader is pointed to the original papers for a detailed description of the ODR, which adopts a reflection coefficient approach rather than impedance-based. This choice is justified by the advantage of handling a bounded variable, facilitating poles numerical stability, and by an intrinsic CFL stability once discretized.

The conversion is achieved through (3) and the resulting reflection coefficient formulation reads:

$$\beta(s) = \beta_\infty + h_1(s) + e^{-s\tau} h_2(s) \tag{6}$$

with β_∞ the bulk reflection coefficient (i.e. the frequency-independent reflection), τ the resonance delay given by the back-and-forth time traveling inside the liner's cavity and each function h_i given by:

$$h_i = \sum_{n\in\mathbb{Z}} \frac{r_k}{s - s_k} + \int_0^\infty \frac{\mu(\xi)}{s+\xi} d\xi \tag{7}$$

The same nomenclature as in the original paper [13] has been kept, identifying with s_k and r_k respectively the complex conjugated pairs of oscillatory poles and weights and with ξ and μ the real diffusive poles and weights. The link with the modified EHR model (5) lies within the calculation of poles and weights, obtained from knowledge of the coefficients a_i and b_i, which can provide exact solution of the impedance model (5). The complete formulation after discretization reads:

$$\begin{aligned}\beta(s) = \beta_\infty + \sum_{n=1}^{N_s} \frac{r_{1,n}}{s - s_n} + \sum_{k=1}^{N_\xi} \frac{\mu_{1,k}}{s+\xi_k} + \\ + e^{-s\tau} \left(\sum_{n=1}^{N_s} \frac{r_{2,n}}{s - s_n} + \sum_{k=1}^{N_\xi} \frac{\mu_{2,k}}{s+\xi_k} \right)\end{aligned} \tag{8}$$

being N_s and N_ξ the number of complex conjugated oscillatory and real diffusive poles, respectively.

The next step consists of converting (8) from Laplacian (frequency-based) to time domain, in order for it to be implemented in a CFD solver and resolve the acoustic absorption alongside the general flow solution. Instead of solving the convolution product in (4), this is done in the ODR method through additional auxiliary functions φ:

$$\begin{aligned}\mathcal{B}(t) = \beta \star u_n(t) = \beta_\infty u_n(t) + \\ + \sum_{k=1}^{N_\xi} \mu_{1,k} \varphi(t, \xi_k) + \sum_{k=1}^{N_\xi} \mu_{2,k} \varphi(t-\tau, \xi_k) + \\ + \sum_{n=1}^{N_s} r_{1,n} \varphi(t, -s_n) + \sum_{n=1}^{N_s} r_{2,n} \varphi(t-\tau, -s_n)\end{aligned} \tag{9}$$

which are solution of the ordinary differential equations:

$$\begin{cases} \partial_t \varphi(t, s_k) = -s_k \varphi(t, s_k) + u_n(t) \\ \varphi(t, 0) = \varphi(0, s_k) = 0 \end{cases} \tag{10}$$

with $t > 0$, $s_k \in (s_k, -\xi_k)$. As a result, as many auxiliary φ functions as the number of poles of the liner discretization are added. At last, the delay effect is converted into a one-dimensional advection problem of the quantity φ convected at the speed of sound c on a length $L_\tau = c/\tau$. A second auxiliary function ψ is introduced, solution of the partial differential equation:

$$\begin{cases} \partial_t \psi(t, s_k, l) = c\, \partial_l \psi(t, s_k, l) \\ \psi(t, s_k, 0) = \varphi(t, s_k) \\ \psi(0, s_k, l) = 0 \end{cases} \tag{11}$$

with $l \in (0, L_\tau)$. This advection must be carried on the fictitious l-space dimension, numerically discretised with an arbitrary number of cells N_C. In the present development, the number of cells is chosen depending on the input N_{PPW}, cell points per wavelength, thus relating it to the maximum frequency to resolve:

$$N_{\text{C}} = N_{\text{PPW}}\, \tau\, f_{max} \tag{12}$$

being N_{PPW} a multiple of 2 to avoid aliasing. A higher order scheme in the advection (such as spectral difference) will require less points per wavelength, while a simpler scheme (like a second order upwind scheme) will demand a higher resolution to not be dissipative. The last value of the mono-dimensional l-space array (at coordinate $l = L_\tau$) is stored in ψ as the delayed φ variable. The final time-domain reflection coefficient model reads:

$$\begin{aligned}\mathcal{B}(t) = \beta \star u_n(t) = \beta_\infty u_n(t) + \\ + \sum_{k=1}^{N_\xi} \mu_{1,k} \varphi(t, \xi_k) + \sum_{k=1}^{N_\xi} \mu_{2,k} \psi(t, \xi_k, L_\tau) + \\ + \sum_{n=1}^{N_s} r_{1,n} \varphi(t, -s_n) + \sum_{n=1}^{N_s} r_{2,n} \psi(t, -s_n, L_\tau)\end{aligned} \tag{13}$$

The overall additional memory cost introduced by this modeling for each concerned boundary mesh cell equals $(N_s.N_\xi)N_C$. A further advantage of using an ODR, is its need of a limited number of poles compared to other purely numerical multipole models, hence reducing the memory and calculation cost.

3. NUMERICAL IMPLEMENTATION

3.1 Characteristic Boundary Conditions in FV

In this work, it has been used a FV-CFD code solving 3D Navier-Stokes (N-S) equations in an integral conservative form, evaluating flux difference at each cell interface. One of the advantages of such formalism is its correct enforcement of wave propagation, which finds ideal the use of Navier-Stokes Characteristic Boundary Conditions (NSCBC), a class of BC analysing the different waves crossing the boundaries. Their original definition and derivation is given in the work of Poinsot and Lele [22]. Rienstra and Hirschberg [23] further suggested their advantage in determining optimal discretization schemes and stability conditions for acoustic problems. Even though first NSCBCs were developed in Cartesian coordinates $\mathbf{x} = (x, y, z)$, in the present solver a generalized boundary surface $\chi = (\chi, \eta, \zeta)$ can be treated. Given the conservative variables in the vector $\mathcal{U}$:

$$\mathcal{U} = \left(\rho, \rho u, \rho v, \rho w, \rho(e + {}^{|u|^2}\!/_2)\right)^\intercal \tag{14}$$

with ρ density, $\mathbf{u} = (u, v, w)^\intercal$ velocity in Cartesian coordinates and ρe gas internal energy, viscous compressible Navier-Stokes equations in conservative form and general-

ized coordinates read:

$$0 = \frac{1}{J}\frac{\partial \mathcal{U}}{\partial t} + \frac{\partial}{\partial \chi}\left(\mathbf{E}\frac{\chi_x}{J} + \mathbf{F}\frac{\chi_y}{J} + \mathbf{G}\frac{\chi_z}{J}\right) + \\ + \frac{\partial}{\partial \eta}\left(\mathbf{E}\frac{\eta_x}{J} + \mathbf{F}\frac{\eta_y}{J} + \mathbf{G}\frac{\eta_z}{J}\right) + \\ + \frac{\partial}{\partial \zeta}\left(\mathbf{E}\frac{\zeta_x}{J} + \mathbf{F}\frac{\zeta_y}{J} + \mathbf{G}\frac{\zeta_z}{J}\right) \tag{15}$$

where J is the Jacobian matrix transporting from generalized to Cartesian coordinates. The fluxes ($\mathbf{E}$, $\mathbf{F}$, $\mathbf{G}$) are sum of convective ($\mathbf{E}_c$, $\mathbf{F}_c$, $\mathbf{G}_c$) and diffusive ($\mathbf{E}_d$, $\mathbf{F}_d$, $\mathbf{G}_d$) fluxes of $\mathcal{U}$ and are given by:

$$\mathbf{E}_c = (\rho u, \rho u^2 + p, \rho uv, \rho uw, u(\rho e + p))^\intercal \tag{16a}$$

$$\mathbf{F}_c = (\rho v, \rho uv, \rho v^2 + p, \rho vw, v(\rho e + p))^\intercal \tag{16b}$$

$$\mathbf{G}_c = (\rho w, \rho uw, \rho vw, \rho w^2 + p, w(\rho e + p))^\intercal \tag{16c}$$

$$\mathbf{E}_d = (0, p + \tau_{(1,1)}, \tau_{(2,1)}, \tau_{(3,1)}, \\ u\tau_{(1,1)} + v\tau_{(2,1)} + w\tau_{(3,1)} + C_T\partial_x T)^\intercal \tag{16d}$$

$$\mathbf{F}_d = (0, \tau_{(1,2)}, p + \tau_{(2,2)}, \tau_{(3,2)}, \\ u\tau_{(1,2)} + v\tau_{(2,2)} + w\tau_{(3,2)} + C_T\partial_y T)^\intercal \tag{16e}$$

$$\mathbf{G}_d = (0, \tau_{(1,3)}, \tau_{(2,3)}, p + \tau_{(3,3)}, \\ u\tau_{(1,3)} + v\tau_{(2,3)} + w\tau_{(3,3)} + C_T\partial_z T)^\intercal \tag{16f}$$

with $\tau_{i,j}$ viscous stress tensor, C_T thermal conductivity and T temperature. By Jacobian matrix transformation, (15) can be recast into:

$$0 = \frac{\partial \mathcal{U}}{\partial t} + \left(\chi_x\frac{\partial \mathbf{E}}{\partial \chi} + \chi_y\frac{\partial \mathbf{F}}{\partial \chi} + \chi_z\frac{\partial \mathbf{G}}{\partial \chi}\right) + \\ + \left(\eta_x\frac{\partial \mathbf{E}}{\partial \eta} + \eta_y\frac{\partial \mathbf{F}}{\partial \eta} + \eta_z\frac{\partial \mathbf{G}}{\partial \eta}\right) + \\ + \left(\zeta_x\frac{\partial \mathbf{E}}{\partial \zeta} + \zeta_y\frac{\partial \mathbf{F}}{\partial \zeta} + \zeta_z\frac{\partial \mathbf{G}}{\partial \zeta}\right) \tag{17}$$

This allows to decompose the system as the sum of the three directions fluxes. Taking as example the flux related to the direction χ, it can be expressed in term of eigenvector and wave strength:

$$\left(\chi_x\frac{\partial \mathbf{E}}{\partial \chi} + \chi_y\frac{\partial \mathbf{F}}{\partial \chi} + \chi_z\frac{\partial \mathbf{G}}{\partial \chi}\right) = \mathbf{P}_{\mathcal{U}}\mathscr{L} \tag{18}$$

where

- $\mathbf{P}_{\mathcal{U}}$ is the transformation matrix from conservative to characteristics variables, or in other words the right eigenvector of the jacobian $\chi_x\mathbf{A} + \chi_y\mathbf{B} + \chi_z\mathbf{C}$ with:

$$\mathbf{A} = \frac{\partial \mathbf{E}}{\partial \mathcal{U}},\ \mathbf{B} = \frac{\partial \mathbf{F}}{\partial \mathcal{U}},\ \mathbf{C} = \frac{\partial \mathbf{G}}{\partial \mathcal{U}}$$

- $\mathscr{L}$ is the strength (or intensity, amplitude) of the characteristic wave and is defined by:

$$\mathscr{L} = \lambda\mathbf{P}_{\mathcal{U}}^{-1}\frac{\partial \mathcal{U}}{\partial \chi} \tag{19}$$

with λ the characteristic velocities, or the eigenvalue diagonal matrix. When λ is positive, the associated waves are going outside the computational domain and can be directly computed from (19). When λ is negative, waves are entering in the domain and additional boundary conditions are required. In the following:

$$\begin{cases} \lambda_1 = \lambda_2 = \lambda_3 = u_n \\ \lambda_4 = u_n + c \\ \lambda_5 = u_n - c \end{cases} \tag{20}$$

being $u_n = \mathbf{u}.\mathbf{n}$ the surface outgoing normal velocity computed as projection in the three dimensions ($\mathbf{n} = n_x, n_y, n_z$). $\lambda_{1,2,3}$ relate to entropy waves, while λ_4 and λ_5 are respectively the forward and backward moving acoustic waves in the normal χ direction. Given the equivalence between equations (17) and (18), the wave strength of the χ-directed convective characteristics can be computed by:

$$\mathscr{L} = \mathbf{P}_{\mathcal{U}}^{-1}\left(\chi_x\frac{\partial \mathbf{E}_c}{\partial \chi} + \chi_y\frac{\partial \mathbf{F}_c}{\partial \chi} + \chi_z\frac{\partial \mathbf{G}_c}{\partial \chi}\right) \tag{21}$$

In the same fashion, *diffusive* flux according to χ and *transverse* fluxes (comprehensive of a convective and a diffusive part on both η and ζ directions) can be defined, alongside with the conservative variables time-variation:

$$\frac{\partial \mathcal{W}}{\partial t} = \mathbf{P}_{\mathcal{U}}^{-1}\frac{\partial \mathcal{U}}{\partial t} \tag{22a}$$

$$\mathcal{D} = \mathbf{P}_{\mathcal{U}}^{-1}\left(\chi_x\frac{\partial \mathbf{E}_d}{\partial \chi} + \chi_y\frac{\partial \mathbf{F}_d}{\partial \chi} + \chi_z\frac{\partial \mathbf{G}_d}{\partial \chi}\right) \tag{22b}$$

$$\mathcal{T} = \mathbf{P}_{\mathcal{U}}^{-1}\left[\left(\eta_x\frac{\partial \mathbf{E}}{\partial \eta} + \eta_y\frac{\partial \mathbf{F}}{\partial \eta} + \eta_z\frac{\partial \mathbf{G}}{\partial \eta}\right) + \\ + \left(\zeta_x\frac{\partial \mathbf{E}}{\partial \zeta} + \zeta_y\frac{\partial \mathbf{F}}{\partial \zeta} + \zeta_z\frac{\partial \mathbf{G}}{\partial \zeta}\right)\right] \tag{22c}$$

A simplified form of conservation equation (17) can now be given:

$$\frac{\partial \mathcal{W}}{\partial t} + \mathscr{L} + \mathcal{D} + \mathcal{T} = 0 \tag{23}$$

3.2 TDIBC implementation

Countless NSCBCs have been developed in the literature, all deriving from the originals in [22] for the most classic boundary types (inlet, outlet, wall, ...). Herein the derivation of the wall condition is reviewed with the purpose of extending it to an acoustically absorbing wall. A no-slip wall sees imposed the three-component velocity null ($\lambda_{1,2,3} = 0$) and leaving the conditions on the exiting and entering acoustic waves (linked to $\lambda_{4,5}$):

$$\begin{cases} \partial_t\mathcal{W}^{in} = \partial_t p - \rho c\partial_t u_n \\ \partial_t\mathcal{W}^{out} = \partial_t p + \rho c\partial_t u_n \end{cases} \tag{24}$$

where with "*out*" is intended the outgoing (or incident) acoustic wave and with "*in* the ingoing (or reflected) acoustic wave. The incident wave can be computed inside the domain, while the hard wall reflection condition gives us the remaining relation to solve in the boundary condition:

$$\partial_t\mathcal{W}^{in} = \partial_t\mathcal{W}^{out} \tag{25}$$

Therefore, an acoustically absorbing surface will dampen the amplitude of the reflected wave by a (reflection) coefficient:

$$\partial_t \mathcal{W}^{in} = \mathcal{B}(\partial_t \mathcal{W}^{out}) \tag{26}$$

For a rigid wall $\mathcal{B} = \mathcal{I}$ (identity matrix), while for a completely absorbing surface $\mathcal{B} = O$ (zero-matrix). It is at this stage that the previously derived TDIBC (13) finds its implementation in the CFD solver. Remembering the relation (23), and recollecting convective ($\mathscr{L} + \mathcal{D}$) and transverse ($\mathcal{T}$) fluxes into a single flux variable ($\mathcal{F}$), this reduces in having:

$$\mathcal{F}^{in} = \mathcal{B}(\mathcal{F}^{out}) \tag{27}$$

hence, developing the $\mathcal{B}$-operator (13) and isolating the convective characteristic wave amplitude entering the domain (i.e. the one to determine, $\mathscr{L}^{in}$):

$$\begin{aligned} \mathscr{L}^{in} = \beta_\infty \mathcal{F}^{out} - (\mathcal{T} + \mathcal{D})^{in} + \\ + \sum_{k=1}^{N_\xi} \mu_{1,k} \varphi_{\xi,k} + \sum_{k=1}^{N_\xi} \mu_{2,k} \psi_{\xi,k} + \\ + \sum_{n=1}^{N_s} r_{1,n} \varphi_{r,n} + \sum_{n=1}^{N_s} r_{2,n} \psi_{r,n} \end{aligned} \tag{28}$$

where φ is dependent on the flux value $\mathcal{F}^{out}$ and ψ is directly obtained through delay of the variable φ. This is valid for purely acoustic problems; however, when a mean flow is considered, the hypothesis of null velocity components $\lambda_{1,2,3} = 0$ falls and the three relative characteristic waves need to be extrapolated from the solution, as they will interact with the flux balance.

4. RESULTS

The present work focuses on the implementation of the TDIBC (13) previously developed by Monteghetti [12] in the *elsA* software in a new fashion. Therefore and for the sake of conciseness, the TDIBC model is assumed correct from the validations carried in [12, 13]. Additional validations have been carried aside by the authors on other liner geometries comparable to those mounted on aircraft engines, and all provided the same quality of results than those found by Monteghetti. The implementation in *elsA* software is herein validated against the benchmark case of Jones *et al.* [24], so the same ODR coefficients set (poles and weights) of Monteghetti have been used (namely $\tilde{\beta}_D$ and $\tilde{\beta}_E$ of Table 2 in ref. [12]), in order to obtain differences only due to the numerical discretization and not to coefficients or model choice.

4.1 1D CFD Validation

A one-dimensional wave reflection in a tube has been used as first validation test, comparing the analytical solution, available for this particular case, with the numerical outcome of the CFD software with TDIBC. The setup consists of a sinusoidal pulse of 1 Pa amplitude with characteristic rightwards velocity $u = p/(\rho c_0)$, initialized in the middle of a 1D tube. The tube's length is adapted to be three times the pulse wavelength. Top and bottom boundaries are symmetry walls, not introducing any transverse effect into the computational domain. Right boundary is an acoustic absorbing wall modeled with the TDIBC (13) and left boundary a non-reflective outlet condition as in (27) with $\mathcal{B}(t) = O$. A probe to capture the pressure signal in time is placed right after the initialized pulse, at the green dot location of Figure 1. The numerical setting is made of an implicit dual-time step marching scheme, a second-order Roe flux reconstruction with third-order limiter resolving Euler equations. Grid and time resolution have been chosen at 40 cells per wavelength and 100 timesteps per period, which showed to be enough to suppress any spurious numerical dissipation. 8 points per wavelength (PPW) have proven sufficient for resolving the delay advection problem with a spectral difference scheme. Figure 2 shows the pressure signal for frequencies of 1.0 and 2.0 kHz. A detailed analysis of the reflected signal shows that the first dampened wave between 2 and 2.5 periods of time comes from the liner's direct sound absorption, while from 2.5 periods onwards the delay effect from the cavity resonance is added, modifying the signal structure. Computational time is barely unaffected by the new TDIBC implementation in this 1D case, since the few additional calculations are done only in the single right boundary cell.

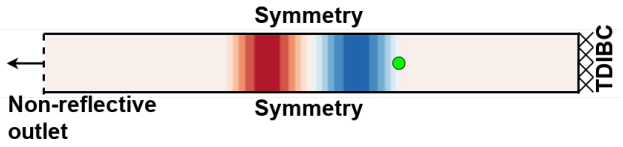

Figure 1: Numerical layout of the 1D case - rightwards moving sinusoidal pulse of 1 Pa amplitude

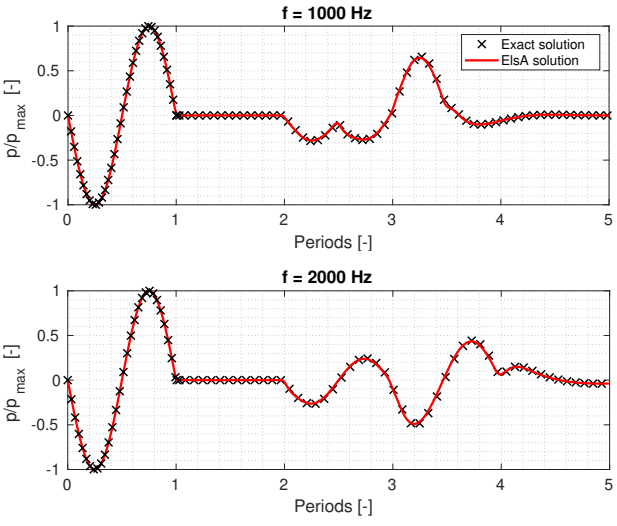

Figure 2: Comparison between analytical and numerical (CFD) results of the 1D reflection case

4.2 2D CFD Validation

A two-dimensional validation has been run aiming at reproducing the experimental results of the aforementioned

benchmark [24]. Geometrical feature of the 2D rectangular duct are as in the original article and the numerical layout is presented in Figure 3. A continuous sinusoidal sound signal of 130 dB is injected from the left side with a reflective characteristic boundary condition (hence taking into consideration incoming waves due to the reflection at the impedance discontinuity) and ejected from the right side with a non-reflective outlet. The TDIBC covers three fifth of the top boundary while all others boundaries are rigid wall. The structured rectangular grid has been sized on the highest frequency 3.0 kHz: 300 $\times$ 35 mesh elements corresponding to approximately 40 points per wavelength in the longitudinal direction. Figures 4a to 4d present successive time frames of the sound signal deformation caused by the TDIBC on the top wall. Immediately after the TDIBC activation, pressure profiles start to deform following the impedance law. After around 10 periods, pressure in the duct reaches a stabilized regime, similarly to the one already obtained after 4 periods. 10 additional periods have been calculated for stability bullet-proofing, for a total of 20 periods time simulation (or 2000 iterations). Six frequencies are herein tested (0.6, 1.0, 1.5, 2.0, 2.5, 3.0 kHz) at two different average Mach numbers (0 and 0.255). The flow profile considered is at this first stage uniform at the given average Mach number. Pressure is extracted at 100 equidistant locations on the opposite wall, as done in the experiment with microphones. Sound Pressure Level (SPL) and its phase are obtained through use of an FFT algorithm on the pressure signal and using the following well-known rule:

$$SPL = 20 \log_{10} \left(\frac{p}{p_{ref}} \right) \tag{29}$$

with $p_{ref} = 20\mu$Pa. Signal phase is presented in Figure 5 (only for the 3.0 kHz case) and showed an impeccable agreement both with experiment and previous DG (Discontinuous Galerkin) CAA calculation of [12]. Comparison in terms of SPL reduction between the experimental values, DG-CAA results and the current CFD implementation are in Figures 6 and 7, respectively for Mach 0 and 0.255. Vertical dashed lines indicate the liner's limits. A great accordance has been found with both references at every frequency. Similar behaviors are found at same excitation frequencies for both velocities, such as the underestimation at 2kHz and 3kHz. This can be justified from using the same grid in all cases, so less points per wavelength at high frequencies. On the other side, the 1000Hz case is correctly resolved with its strong absorption of almost 50 dB.

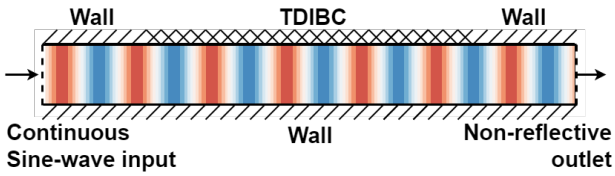

Figure 3: Numerical layout of the 2D case - continuous sinusoidal sound signal of 130 dB amplitude

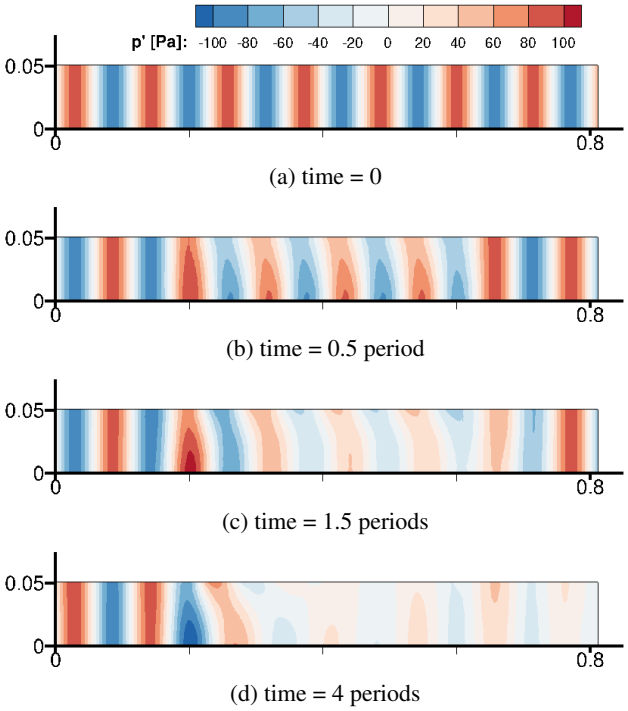

Figure 4: 2D pressure time-evolution in the duct

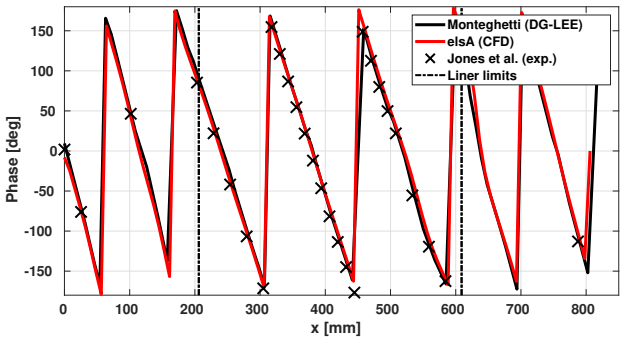

Figure 5: Phase comparison for the fundamental frequency only (3000 Hz)

5. CONCLUSION

The implementation of a time-domain impedance boundary condition in a Finite Volume CFD solver has been presented. Different validation cases proved its excellent behaviour, both in terms of phase and sound level prediction. The additional computational time and memory have been kept to minimal acceptable values. At the present stage, the aforementioned model can be used to predict linear liners behaviour for different frequencies and geometries. The most evident progress on this subject is the extension of the $\mathcal{B}$-model to non-linearly reacting liners and nonlinear physics, like shock waves propagation in fan inlets, where the high SPL variations can influence the acoustic reaction of the material. Even though many studies on non-linear wave propagation can be already found in literature, very little has been done about non-linear liners integrated in non-linear environments, where models are expected to be formulated in abscene of analytical expressions.

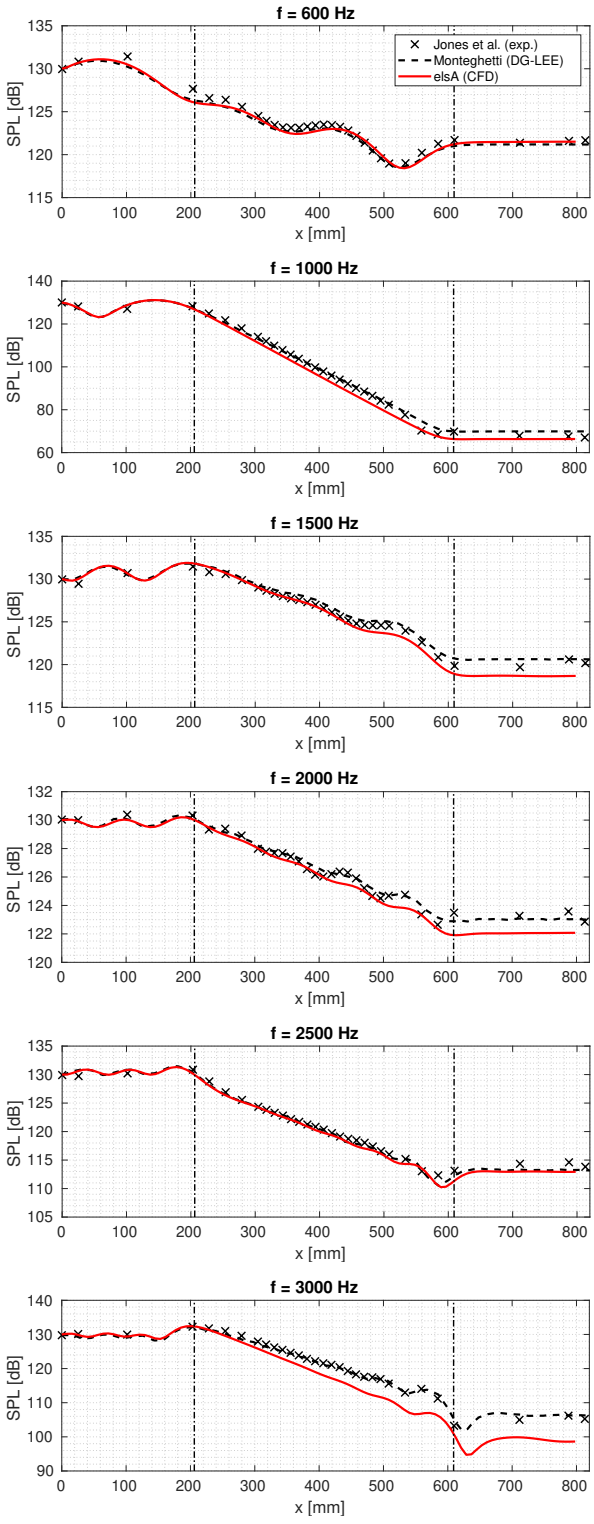

Figure 6: SPL comparison of experiment, CAA-DG and the herein developed CFD (*elsA*) - average Mach = 0

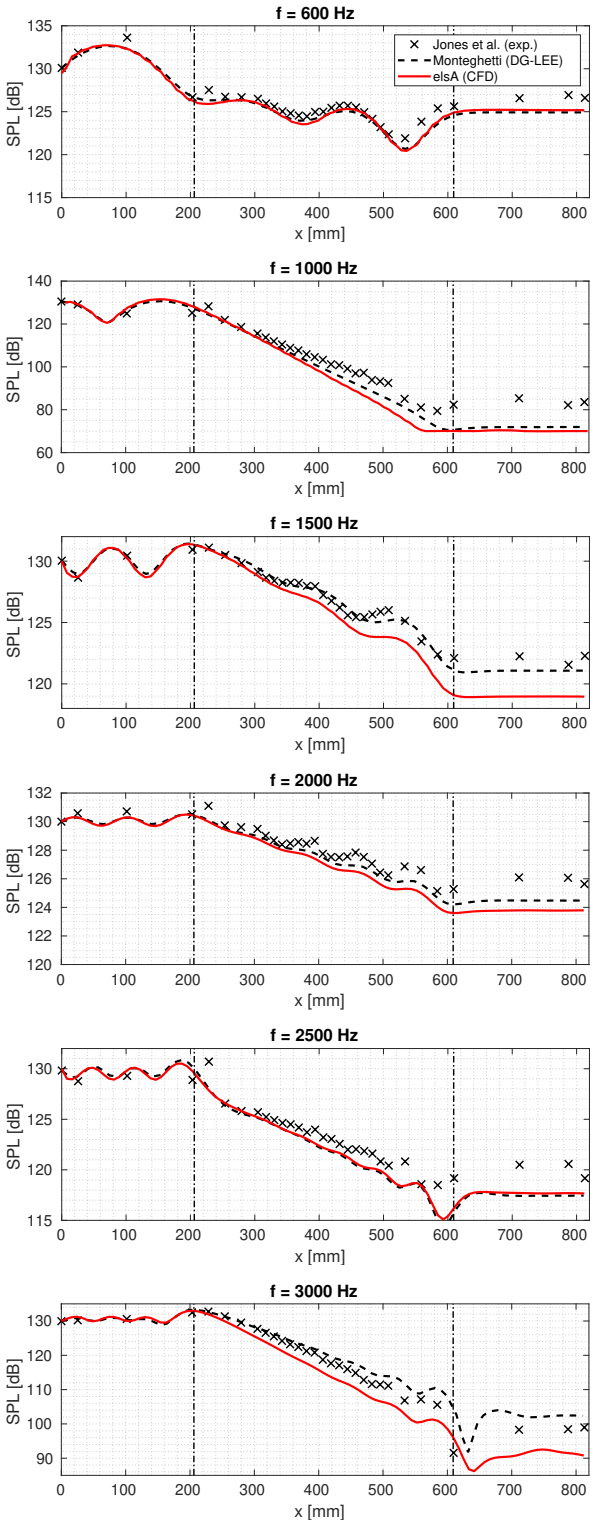

Figure 7: SPL comparison of experiment, CAA-DG and the herein developed CFD (*elsA*) - average Mach = 0.255

6. ACKNOWLEDGEMENTS

The first author thanks Airbus Operations S.A.S. and ANRT for financing the work under the Ph.D. CIFRE contract n°2018/0772, and Onera for the fundamental technical support. The solver used in the present work is *elsA* (**e**nsemble **l**ogiciel de **s**imulation **a**érodynamique, software package for aerodynamic simulation), jointly developed by Onera, Safran and Airbus. The authors are also grateful to Michael G. Jones for providing the experimental database used for validating the results herein achieved. The first author finally thanks Romain Fiévet for his guidance.

7. REFERENCES

[1] C. K. W. Tam and L. Auriault, "Time-domain impedance boundary conditions for computational aeroacoustics," *AIAA Journal*, vol. 34, no. 5, pp. 917–923, 1996.

[2] Y. Özyörük and L. N. Long, "A time-domain implementation of surface acoustic impedance condition with and without flow," *Journal of Computational Acoustics*, vol. 05, no. 3, pp. 277 – 296, 1997.

[3] Y. Özyörük, L. N. Long, and M. G. Jones, "Time-domain numerical simulation of a flow-impedance tube," *Journal of Computational Physics*, vol. 146, no. 1, pp. 29 – 57, 1998.

[4] B. Van den Nieuwenhof and J.-P. Coyette, "Treatment of frequency-dependent admittance boundary conditions in transient acoustic finite/infinite-element models," *The Journal of the Acoustical Society of America*, vol. 110, pp. 1743–51, 11 2001.

[5] S. Rienstra, "Impedance models in time domain, including the Extended Helmholtz Resonator model," *Collection of Tech. Papers - 12th AIAA/CEAS Aeroacoustics Conference*, vol. 6, 2006.

[6] K. Fung and H. Ju, "Broadband time-domain impedance models," *AIAA Journal*, vol. 39, no. 8, pp. 1449–1454, 2001.

[7] K.-Y. Fung and H. Ju, "Time-domain impedance boundary conditions for computational acoustics and aeroacoustics," *International Journal of Computational Fluid Dynamics*, vol. 18, no. 6, pp. 503–511, 2004.

[8] Y. Reymen, M. Baelmans, and W. Desmet, "Time-domain impedance formulation based on recursive convolution," in *12th AIAA/CEAS Aeroacoustics Conference (27th AIAA Aeroacoustics Conference)*.

[9] Y. Reymen, M. Baelmans, and W. Desmet, "Time-domain acoustic simulation of 3D lined ducts with flow using an unstructured Discontinuous Galerkin method," in *14th International Congress on Sound and Vibration 2007*, vol. 4, 01 2007.

[10] X. Y. Li, X. D. Li, and C. K. W. Tam, "Improved multipole broadband time-domain impedance boundary condition," *AIAA Journal*, vol. 50, no. 4, pp. 980–984, 2012.

[11] R. Troian, D. Dragna, C. Bailly, and M.-A. Galland, "Broadband liner impedance eduction for multimodal acoustic propagation in the presence of a mean flow," *Journal of Sound and Vibration*, vol. 392, pp. 200–216, 2017.

[12] F. Monteghetti, D. Matignon, and E. Piot, "Energy analysis and discretization of nonlinear impedance boundary conditions for the time-domain linearized euler equations," *Journal of Computational Physics*, vol. 375, pp. 393 – 426, 2018.

[13] F. Monteghetti, D. Matignon, E. Piot, and L. Pascal, "Design of broadband time-domain impedance boundary conditions using the oscillatory-diffusive representation of acoustical models," *The Journal of the Acoustical Society of America*, vol. 140, pp. 1663–1674, 2016.

[14] C. Scalo, J. Bodart, and S. K. Lele, "Compressible turbulent channel flow with impedance boundary conditions," *Physics of Fluids*, vol. 27, no. 3, p. 035107, 2015.

[15] Q. Douasbin, C. Scalo, L. Selle, and T. Poinsot, "Delayed-time domain impedance boundary conditions (d-tdibc)," *Journal of Computational Physics*, vol. 371, 05 2018.

[16] R. Fiévet, H. Deniau, and E. Piot, "Strong compact formalism for characteristic boundary conditions with discontinuous spectral methods," *Journal of Computational Physics*, p. 109276, 2020.

[17] M. O. Burak, M. Billson, L.-E. Eriksson, and S. Baralon, "Validation of a time- and frequency-domain grazing flow acoustic liner model," *AIAA Journal*, vol. 47, no. 8, pp. 1841–1848, 2009.

[18] M. Shur, M. Strelets, A. Travin, T. Suzuki, and P. R. Spalart, *Unsteady Simulation of Sound Propagation in Turbulent Flow Inside a Lined Duct Using a Broadband Time-Domain Impedance Model*. 2020.

[19] D. Dragna, P. Pineau, and P. Blanc-Benon, "A generalized recursive convolution method for time-domain propagation in porous media," *The Journal of the Acoustical Society of America*, vol. 138, no. 2, pp. 1030–1042, 2015.

[20] M. Bruneau, *Fundamental of Acoustics*. London: ISTE Ltd, 2006.

[21] I. B. Crandall, *Theory of Vibrating Systems and Sound*. D. Van Nostrand Company, 1926.

[22] T. Poinsot and S. Lele, "Boundary conditions for direct simulations of compressible viscous flows," *Journal of Computational Physics*, vol. 101, no. 1, pp. 104 – 129, 1992.

[23] S. Rienstra and A. Hirschberg, *An introduction to acoustics*. Eindhoven University of Technology, 2018.

[24] M. Jones, W. Watson, and T. Parrott, "Benchmark data for evaluation of aeroacoustic propagation codes with grazing flow," in *11th AIAA/CEAS Aeroacoustics Conference*, 2005.